remote sensing

MDPI

Article

Combining Electrical Resistivity Tomography and Satellite Images for Improving Evapotranspiration Estimates of Citrus Orchards

Daniela Vanella [1], Juan Miguel Ramírez-Cuesta [2,*], Diego S. Intrigliolo [2] and Simona Consoli [1]

[1] Dipartimento di Agricoltura, Alimentazione, Ambiente (Di3A), Università degli Studi di Catania, Via S. Sofia, 100–95123 Catania, Italy; d.vanella@unict.it (D.V.); simona.consoli@unict.it (S.C.)

[2] Dpto. Riego, Centro de Edafología y Biología Aplicada del Segura (CEBAS-CSIC), P.O. Box 164, 30100 Murcia, Spain; dintri@cebas.csic.es

* Correspondence: ramirezcuesta.jm@gmail.com; Tel.: +34-699-689673

Received: 29 December 2018; Accepted: 11 February 2019; Published: 13 February 2019

Abstract: An adjusted satellite-based model was proposed with the aim of improving spatially distributed evapotranspiration (ET) estimates under plant water stress conditions. Remote sensing data and near surface geophysics information, using electrical resistivity tomography (ERT), were used in a revised version of the original dual crop coefficient (K_c) FAO-56 approach. Sentinel 2-A imagery were used to compute vegetation indices (VI_s) required for spatially estimating ET. The potentiality of the ERT technique was exploited for tracking the soil wetting distribution patterns during and after irrigation phases. The ERT-derived information helped to accurately estimate the wet exposed fraction (f_{ew}) and therefore the water evaporated from the soil surface into the dual K_c FAO-56 approach. Results, validated by site-specific ET measurements (ET_{EC}) obtained using the eddy covariance (EC) technique, showed that ERT-adjusted ET estimates (ET_{ERT}) were considerably reduced (15%) when compared with the original dual K_c FAO-56 approach (ET_{FAO}), soil evaporation overestimation being the main reason for these discrepancies. Nevertheless, ET_{FAO} and ET_{ERT} showed overestimations of 64% and 40% compared to ET_{EC}. This is because both approaches determine ET under standard conditions without water limitation, whereas EC is able to determine ET even under soil water deficit conditions. From the comparison between ET_{EC} and ET_{ERT}, the water stress coefficient was experimentally derived, reaching a mean value for the irrigation season of 0.74. The obtained results highlight how new technologies for soil water status monitoring can be incorporated for improving ET estimations, particularly under drip irrigation conditions.

Keywords: sentinel data; near surface geophysics; irrigation; eddy covariance; soil water balance

1. Introduction

Soil surface evaporation (E) and crop transpiration (T) play a crucial role in terrestrial water balance. Their estimation results are critical for understanding crop water use efficiency (WUE) and improving decision-making for soil and crop water management [1–3]. In this sense, improving the methods used for determining these components (T and E) is needed. While T represents the water used directly by crops, E is considered as an unproductive portion of WUE, which can range from 10% [4] to 59% [5] of the seasonal water balance. In general, two strategies are addressed with the aim of enhancing WUE: (i) increase T or; (ii) reduce E losses. Numerous authors have proposed different mechanisms to increase the proportion of water that is transpired by crop rather than E losses, including: early sowing [6,7], enhancing crop vigorousness [8,9], using narrow row spacing [10],

applying high plant densities [11], and adopting mulching, stubble retention, and a proper weed management [12,13].

Evapotranspiration (ET), which consists of the sum up of both T and E components, can be determined at different spatial and temporal resolutions through different techniques (e.g., lysimeter; eddy covariance, EC; scintillometry). However, partitioning among E and T components is not an easy task. For this reason, it is usual to resort to models, such as the FAO-56 approach [14], which is used as reference. This model includes a simple approach (single crop coefficient, K_c), where T and E are considered together, and a more complex methodology (dual K_c FAO-56), where both T and E components are determined separately (i.e., basal crop coefficient K_{cb} and evaporation coefficient K_e). Both models can be combined with spectral data provided using remote sensors in order to provide spatially distributed ET estimates [15]. Although K_{cb} represents a specific crop characteristics index that varies only to a limited extent with climate, K_e can vary considerably depending on the time interval between wetting events, the magnitude of the wetting event, and the E power of the atmosphere. Nevertheless, these aspects are not deeply addressed in the FAO-56 approach. Thus, the use of alternative techniques is required in order to obtain more accurate K_e estimates.

Moreover, the calculation of K_e needs to take into account the spatial and temporal distribution of irrigation-wetting patterns that are governed by static and dynamic conditions, such as soil characteristics (e.g., hydraulic parameters, texture, structure, initial water content), irrigation systems (types, emitter spacing, discharge rate, and irrigation frequency), and root distribution. In general, soil wetting patterns can be obtained using in situ soil water (SW) measurements. Caution needs to be applied on the use of SW measurements, since site conditions (compaction layers or surface soil conditions) may be quite site-specific, and installation of instrumentation can affect the soil wetting patterns being measured [16]. Undisturbed methods, such as dye tracers, often combined with flow and/or transport modeling, have been used to describe infiltration from a point/line source; however, models do not at present fully reflect the current state of process understanding and empirical knowledge of preferential flow [17]. A number of near surface geophysics methods have been adopted for image irrigation wetting patterns [18]. Among these minimally invasive methods, electrical resistivity tomography (ERT) has the main advantage of being sensitive in monitoring soil-plant interactions in terms of SW relationships with high-resolution scale both in two and/or three dimensions [19–22]. Furthermore, ERT can provide useful information on soil wetting patterns both spatially and temporally distributed if applied in time-lapse mode.

Therefore, the main objective of this work was to explore the potentialities of incorporating ERT derived surface wetting patterns into a satellite-based dual K_c FAO-56 approach for estimating E and assessing its influence on ET by comparison with EC measurements.

2. Materials and Methods

In this study, the assessment of an updated satellite-based procedure based on a dual K_c FAO-56 approach is proposed. A schematic summary of the adopted methodology is reported in Figure 1.

The original satellite dual K_c FAO-56 approach [14] was adjusted with ERT-derived data that provided site-specific information on the exposed wetting fraction (f_{ew}). This parameter represents the fraction of soil that is both exposed and wetted (from which most evaporation occurs). As reported in [14], f_{ew} contributes in the definition of the soil evaporation coefficient (K_e, Equation (2)) and as well in ET determination (see Equation (1)). ERT surveys provided f_{ew} that was incorporated as a parameter into the soil water balance (SWB) model (Equation (4)) within the dual K_c FAO-56 approach, permitting the obtainment of an ERT-adjusted evaporation coefficient ($K_{e,ERT}$) and evapotranspiration estimates (ET_{ERT}).

A validation of ET estimates obtained using both the original dual K_c FAO-56 (ET_{FAO}) and the ERT-adjusted model (ET_{ERT}) was performed with EC-based ET measurements (ET_{EC}) collected in situ. In the following sub-sections, the materials and methods are described in detail.

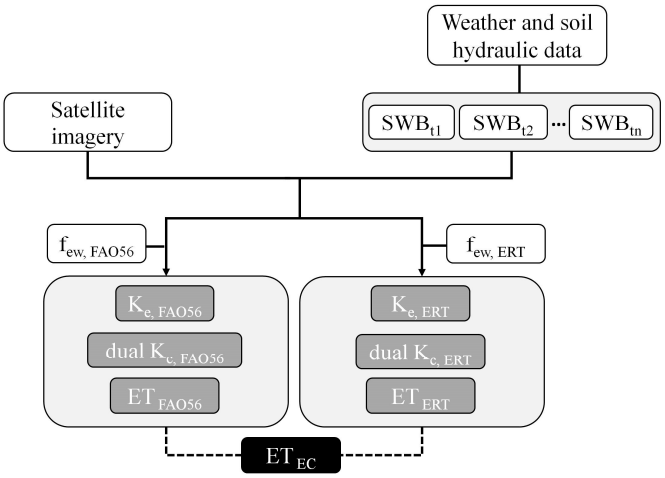

Figure 1. Scheme of the methodology applied in this study.

2.1. Original Model Description

The original dual K_c FAO-56 approach determines crop evapotranspiration (ET_{FAO}) based on the concepts of reference evapotranspiration (ET_0) and separate coefficients for crop T (represented by the basal crop coefficient, K_{cb}) and E (K_e), as follows:

$$ET_{FAO} = (K_{cb} + K_e) \cdot ET_0 \quad (1)$$

where ET_0 (mm d^{-1}) is estimated by using the Penman–Monteith equation with hourly weather data (see 1.2) supplied by a weather station located close to the study site.

K_e depends on the water available in the surface layer of the topsoil and its estimation requires a daily water balance (SWB) computation for the surface soil layer in order to determine the cumulative E or depletion from the wet condition, as follows:

$$K_e = K_r(K_{c,max} - K_{cb}) \quad (2)$$

where $K_{c,max}$ is the maximum crop coefficient value following rain or irrigation while K_r represents the reduction applied to E depending on the amount of water evaporated from the soil, as follows:

$$K_r = \frac{TEW - D_{e,i}}{TEW - REW} \quad (3)$$

where TEW = 1000 ($\theta_{FC} - 0.5\ \theta_{WP}$) Z_e is the total evaporable water (i.e., maximum depth of water that can be evaporated from the soil surface layer), with θ_{FC} and θ_{FC} measured soil field capacity and wilting point (see 2.3) at the study site and Z_e equal to 0.1, as reported in [14]; REW is the readily evaporable water (fixed at 10 mm for the study site soil, i.e., sandy loam [14]); and $D_{e,i}$ is the cumulative depth of evaporation from the topsoil (mm) at the end of the 1-th day, and it is solved as follows:

$$D_{e,i} = D_{e,i-1} - (P_i - RO_i) - \frac{I_i}{f_w} + \frac{E_i}{f_{ew}} + T_{ew,i} + DP_{e,i} \quad (4)$$

where $D_{e,i-1}$ is the cumulative depth of E following complete wetting from the exposed and wetted fraction of the topsoil at the end of day $i - 1$ (mm); P_i is precipitation on day i (mm); RO_i is precipitation runoff from the soil surface on day i (mm); I_i is irrigation depth on day i that infiltrates the soil (mm); E_i is evaporation on day i (i.e., $E_i = K_e\ ET_0$) (mm); $T_{ew,i}$ is depth of T from the exposed and wetted fraction of the soil surface layer on day i (mm); $DP_{e,i}$ is deep percolation loss from the topsoil layer on day i if SW exceeds θ_{FC} (mm); f_w is the fraction of soil surface wetted by irrigation (0.35 for drip irrigation [14]); f_{ew} is exposed and wetted soil fraction, computed as the lowest value between the average exposed

soil fraction not covered (or shaded) by vegetation and f_w [14]. Therefore, f_{ew} calculation within the SWB depends also on the occurrence of irrigation and precipitation and it is calculated differently for each scenario as: (1) if the surface is wetted by irrigation, then f_w is the f_w for the irrigation system, and therefore f_{ew} is equal to 0.35 (this value is obtained from [14]); (2) if the surface is wetted by significant rain (i.e., >3 to 4 mm) with no irrigation, $f_w = 1$ and therefore f_{ew} is $(1 - f_c)$; and (3) if there is neither irrigation nor significant precipitation, f_{ew} is the f_{ew} of the previous day. However, the value of 0.35 considered in this approach, as it is a general theoretical f_{ew} procedure, may not reflect the site-specific conditions, which could be more accurately determined performing local measurements (as the ERT-adjustment described in Section 2.2 "ERT-adjusted model parameter").

2.2. ERT-Adjusted Model Parameter

As stated in Section 2.1, f_{ew} values proposed in [14] can be adjusted in order to account for the site specificities (such as soil type and depth, and dripper flow and density, among others). This is the case of the novel ERT-adjusted dual K_c FAO-56 approach proposed herein. In this approach, $K_{r,ERT}$ (Equation (3)) and $K_{e,ERT}$ (Equation (2)) were calculated by solving the SWB model (Equation (4)) using the f_{ew} information provided by ERT instead of using the FAO-56 proposed f_{ew} value as in the original FAO-56 model, thus ET_{ERT} was derived by including the modified $K_{e,ERT}$ term in Equation (1).

ERT (see [23]) is an active source geophysical method that uses a low-frequency electrical current, galvanically injected into the ground between a pair of current source electrodes, and measures the potential between two or more different potential electrodes. A cross section or a volume distribution of electrically resistive or conductive regions in the subsurface is the result obtained by repeating the patterns through many combinations of transmitting and receiving electrodes along a line or grid (or with borehole electrodes). The current, voltage, electrode spacing, and electrode configuration are used to calculate the electrical resistivity (ER, i.e., the inverse of electrical conductivity).

ERT surveys were carried out in 2017 (15th and 18th September) at the experimental site. A three-dimensional (3-D) set-up (made of 72 surface and borehole electrodes) was used to monitor the unsaturated soil volume (1.3 × 1.3 × 1.2 m) around the root-zone of two trees, one irrigated by micro-drippers at full rate, T1, and the other one supplied at 50% of T1 by PRD strategy, T2. A full description of the 3-D ERT set-up and data processing is reported in [22].

The electrical resistance (ohm, Ω) dataset was collected at T1 and T2, with short-term repetitions during and after irrigation phases, in order to get dynamic information about sub-surface processes (for further details refer to [24]). Table 1 displays the acquisition time during the irrigation phase for T1 and T2.

Table 1. Three-dimensional (3-D) electrical resistivity tomography (ERT) data collection time (local time).

		T1		T2	
Time Id	**State**	**Starting Time**	**Ending Time**	**Starting Time**	**Ending Time**
00	no irrigation	9.17	9.46	9.29	10.02
01	during the irrigation phase	10.42	11.11	11.01	11.35
02		11.39	12.09	11.58	12.30
03	after the irrigation phase	12.55	13.24	12.57	13.30
04		13.47	14.16	13.52	14.24
05		14.41	15.09	14.43	15.17

Time-lapse inversions were adopted to produce images of ER changes (ER ratio in %) before, during, and after irrigation phase. These relative inversions (time-lapse) are calculated from ratios (d_r, Equation (5)) between the electrical resistances collected before and after irrigation:

$$d_r = \frac{d_t}{d_0} \cdot F(\sigma_{ohm}) \quad (5)$$

where d_t and d_0 are the electrical resistance values (Ω) at time t and time 0 (initial condition), and $F(\sigma_{ohm})$ is the electrical resistance (Ω), obtained by running the forward model for an arbitrary ER of 100 Ω m. This calculation was performed simultaneously for T1 and T2 using a 5% error level [22].

Soil wetting distribution patterns (i.e., surface and depth of the soil layer dried by E) were identified based on ER decreasing in respect to the initial condition (no irrigation) by applying a threshold corresponding to a reduction in ER equal to or greater than 10%.

The f_{ew} parameter used to set the SWB model (Equation (4)) within the ERT-adjusted dual K_c FAO-56 approach was retrieved from the volume derived by ERT. From the entire volume, the ER ratio values corresponding uniquely to the first 10 cm were extracted, since it was assumed that it is mainly at this depth where soil evaporation occurs. Once the data corresponding to the first 10 cm were extracted, f_{ew} was determined by recognizing the soil wetting patterns (i.e., extracting all the values corresponding to the fixed threshold) at the different acquisition times after the irrigation beginning (Figure 2a and Table 1). Finally, the constant f_{ew} value used in the ERT-adjusted approach was obtained as an average of all instantaneous values retrieved in each acquisition time (Figure 2a and Table 1).

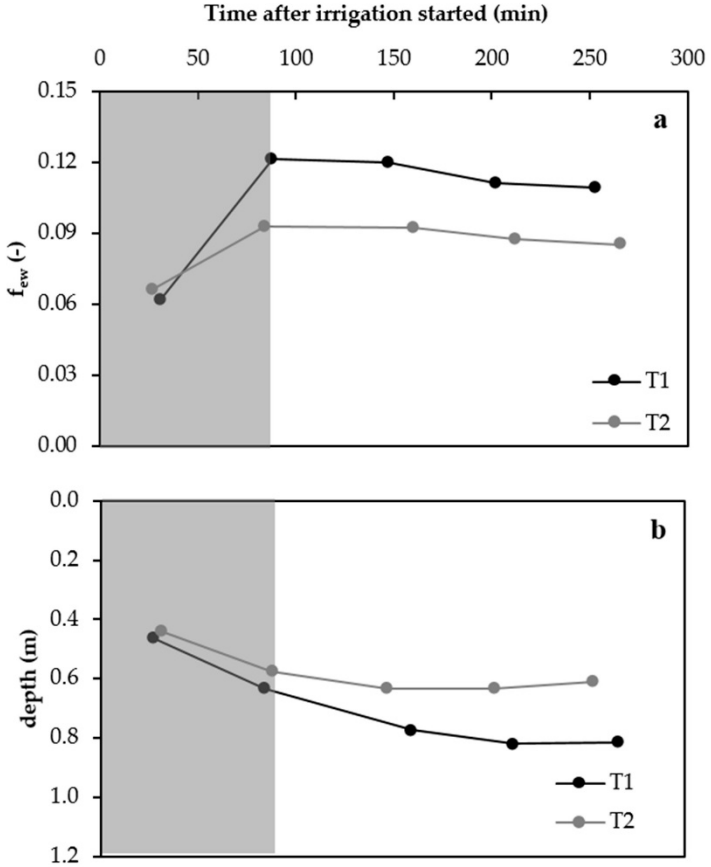

Figure 2. Evolution of the exposed wetted area (f_{ew}) (**a**) and evolution of the infiltration front depth (m) in T1 and T2 during and after an irrigation phase (**b**). Time is expressed in minutes after the irrigation start. The grey area represents the irrigation phase period.

2.3. Satellite-Based Dual Kc Approach

The dual K_c FAO-56 approach (original and ERT-adjusted), applied in this study, incorporates data derived from remote sensing in order to obtain spatially distributed estimates of K_e ($K_{e,FAO}$ and $K_{e,ERT}$), K_{cb} (Equations (2) and (6)), and ET (ET_{FAO} and ET_{ERT}) (Equation (1)).

Sentinel 2-A (L-1C) data offered by the European Space Agency (ESA), with a spatial resolution of 10 m in the visible and near-infrared (VNIR) region and available every 10 days, were selected on the basis of clear sky condition and irrigation application.

Table 2 displays the dates of the satellite imagery used within the reference period June–September 2017.

Table 2. Sentinel images used in the study.

Acquisition Dates	Day of the Year (DOY)
7 June 2017	158
27 June 2017	178
12 July 2017	193
17 July 2017	198
1 August 2017	213
6 August 2017	218
11 August 2017	223
16 August 2017	228
26 August 2017	238
5 September 2017	248
15 September 2017	258

Remote sensing data were used to determine K_{cb} (Equations (1) and (2)) as a function of the soil adjusted vegetation index (SAVI) following the methodology proposed by [25,26]:

$$K_{cb} = \frac{K_{cb,max}}{F_{c,max}} \left(\frac{SAVI - SAVI_{min}}{SAVI_{max} - SAVI_{min}} \right) \quad (6)$$

where $SAVI_{max}$ and $SAVI_{min}$ refer to the maximum and minimum SAVI values for each image, and $F_{c,max}$ is the maximum value of fractional vegetation cover (f_c) within the study site for which K_{cb} reaches its maximum value (as in [14]).

The SAVI index is calculated as follows:

$$SAVI = \left(\frac{\rho_{NIR} - \rho_{RED}}{\rho_{NIR} + \rho_{RED} + L} \right) (1 + L). \quad (7)$$

where ρ_{NIR} and ρ_{RED} are the infrared and red reflectance of Sentinel images and L is a soil normalization factor, generally taken to be 0.5 [27].

In order to compute $F_{c,max}$ (Equation (6)) and f_{ew} [14], f_c is calculated as reported in [28]:

$$f_c = \left(\frac{NDVI - NDVI_{min}}{NDVI_{max} - NDVI_{min}} \right) \quad (8)$$

with NDVI derived from Sentinel reflectance data as NDVI = $(\rho_{NIR} - \rho_{RED})/(\rho_{NIR} + \rho_{RED})$ [29]. The value of $NDVI_{max}$ (set to 1) corresponds with the NDVI when f_c is maximum ($f_c = 1$) whereas $NDVI_{min}$ (set to 0) refers to the NDVI value when the surface is without vegetation ($f_c \approx 0$). Within the study period, the f_c at the study site ranged between 0.337 and 0.646, with an average value of 0.483.

2.4. Ancillary Weather and Soil Data

The ground-based information implemented into the dual K_c FAO-56 model consists of weather observations and soil hydraulic characteristics referring to an experimental orange orchard of 0.7 ha located in southern Italy (Lentini, SR) and managed by Centro di Ricerca Olivicoltura, Frutticoltura e Agrumicoltura of the Italian Council for Agricultural Research and Agricultural Economics Analyses (CREA-OFA, Acireale). The orange orchard has been treated by deficit irrigation strategies, including partial root-zone drying (PRD) and regulated deficit irrigation (RDI), since 2010. The complete description of the experimental site and the irrigation strategies applied are reported in [21,30,31].

Hourly and daily weather data were provided by a meteorological station (37.35°N, 14.91°E, 50 m a.s.l.) located about 2 km from the experimental site and managed by Servizio Informativo Agrometeorologico Siciliano (SIAS; www.sias.regione.sicilia.it).

Weather data (air temperature, T_{air}, °C; relative humidity, RH, %; precipitation, P, mm; wind speed, u, m s^{-1}; and reference evapotranspiration, ET_0, mm), were analyzed in order to initiate/calibrate and implement the SWB model within the dual K_c FAO-56 model.

The temporal evolution of the main weather parameters (ET_0, maximum T_{air} and P) is shown in Figure 3.

The soil hydraulic parameters (i.e., θ_{FC} = 0.28 m^3 m^{-3} and θ_{WP} = 0.14 m^3 m^{-3}) were obtained by laboratory analyses on soil samples collected at the experimental site [21,32] and incorporated into the SWB model within the dual K_c FAO-56 approach.

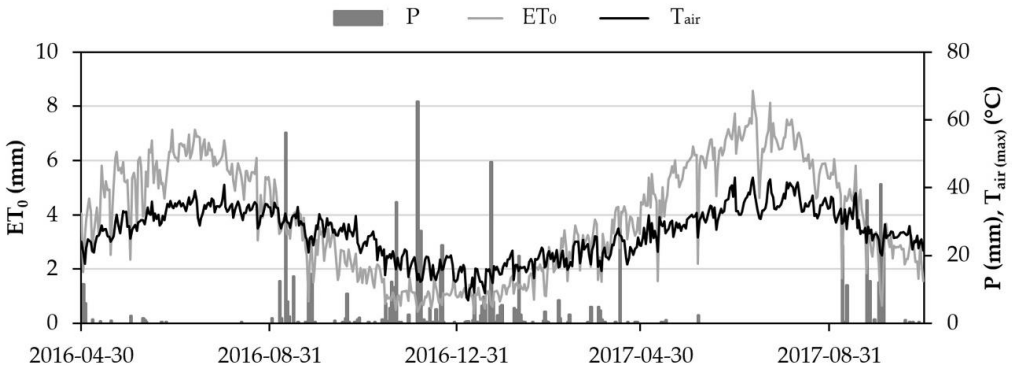

Figure 3. Temporal evolution of weather parameters used to implement the soil water balance (SWB) model within the dual K_c FAO-56 approach. Values refer to the reference period (April 2016–October 2017). P is the precipitation (mm); ET_0 is the reference evapotranspiration (mm); and T_{air} is the air temperature (°C).

2.5. Evapotranspiration Validation Using EC

The eddy covariance (EC) method is a direct measurement of a turbulent flux density of a scalar across horizontal wind streamlines [33]. At the experimental site, an EC system is mounted on a tower at 7 m above the surface (about two times the canopy height). The EC system consisted of a three-dimensional sonic anemometer (CSAT3-3D, Campbell Scientific Inc.) and an infrared open-path gas analyzer (Li-7500, Li-cor Biosciences Inc.) to obtain high frequency measurements of the three wind components and the H_2O and CO_2 concentrations, respectively. The sample frequency for the raw data was 10 Hz (high frequency data) [31]. Low frequency data (30-min) were obtained for: net radiation (R_n, W m^{-2}, net radiometer CNR-1 Kipp & Zonen, located 7 m above the ground) and soil heat flux (G, W m^{-2}), obtained using self-calibrated soil heat flux plates (HFP01SC, Hukseflux) placed in the exposed, half-exposed, and shadowed soil at a depth of about 0.05 m.

High and low frequency data were recorded and stored in a CR1000 logger (Campbell Scientific Inc.).

EC permits to obtain ET rates (ET_{EC}) by the direct measurements of latent heat flux (λET, W m^{-2}) exchanged within the soil-plant-atmosphere continuum, using the following equation:

$$\lambda ET_{EC} = \lambda \cdot \sigma_{wq} \quad (9)$$

where λ (J g^{-1}) is the latent heat of vaporization and σ_{wq} (g m^{-2} s^{-1}) is the covariance between the vertical wind speed and water vapour density.

EC sensible heat flux (H, W m^{-2}) is computed as:

$$H = \rho \cdot c_p \cdot \sigma_{wT} \quad (10)$$

where ρ (g m^{-3}) is the air density, c_p (1004 J g^{-1} K^{-1}) is the air specific heat capacity at constant pressure, and σ_{wT} (m s^{-1} K) is the covariance between the vertical wind speed and air temperature.

The standard EUROFLUX rules [34] were adopted for EC measurements and data processing. Common errors in the measured high frequency data, such as running means for detrending, three angles coordinate rotations, and despiking, were removed during the post processing by quality checks. The stationarity of the surface flux layer and the surface energy balance closure were also evaluated [35]. The surface energy balance closure ratio (*CR*) is expressed as:

$$CR = \frac{(H + \lambda ET)}{(R_n - G)} \quad (11)$$

and allows for determining how well the turbulent fluxes of heat and water vapor account for the available energy. The ratio, as suggested by [36], was performed only when R_n is greater than 100 W m^{-2}. In this study, the *CR* was forced according to the procedure proposed by [37], in order to maintain the observed Bowen ratio between *H* and LE as constant.

Thirty-minute fluxes data were aggregated to a daily scale, and latent heat fluxes, acquired in W m^{-2}, were then transformed to equivalent depth of ET (mm d^{-1}). In this study, ET_{EC} measurements were used as a reference to compare the ET estimates obtained by the original satellite-based dual K_c FAO-56 (ET_{FAO}) approach and the ET estimates (ET_{ERT}) obtained by the adjusted model with ERT-derived parameters (f_{ew}).

Using the ET_{EC} measures (mm d^{-1}) and ET_0 by weather station (mm d^{-1}), the crop coefficient using EC ($K_{c,EC}$) was estimated, as in the following:

$$K_{c,EC} = \frac{ET_{EC}}{ET_0}. \quad (12)$$

2.6. Water Stress Coefficient Determination

The above described dual K_c FAO 56 approaches (both the original and ERT-adjusted) compute ET under standard conditions (i.e., water stress coefficient, K_s, equal to 1), whereas ET measured using the EC technique (ET_{EC}) incorporates soil water stress condition ($ET_{EC} = K_s\ K_{c,EC}\ ET_0$; $K_{c,EC}$ being the hypothetical K_c value that will be measured by EC in the absence of water stress). Thus, assuming that $K_{c,ERT}$ is equal to $K_{c,EC}$, K_s can be empirically derived as:

$$K_s = \frac{ET_{EC}}{ET_{ERT}} = \frac{K_s \cdot K_{C,EC} \cdot ET_0}{K_{cERT} \cdot ET_0}. \quad (13)$$

3. Results

3.1. Evapotranspiration Rates using EC

The temporal evolution of daily scale ET_{EC} rates within the reference period (June–September 2017) is shown in Figure 4. ET_{EC} rates ranged between 0.94 and 3.50 mm day^{-1}, with a mean value of 2.24 mm d^{-1}. Prior to the CR adjustment, the slope of the regression forced through the origin of the CR was around 0.82, with a determination coefficient (R^2) of about 0.90.

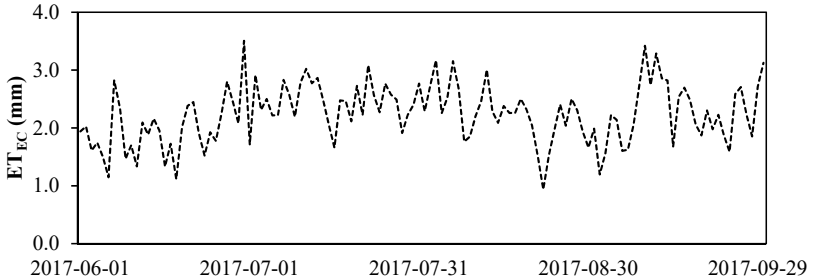

Figure 4. Temporal evolution of daily evapotranspiration measurements (ET_{EC}) rates using eddy covariance (EC).

3.2. Soil Wetting Distribution Patterns Using ERT

Figures 5 and 6 show the changes in ER ratio (at the surface: a–e; transects under the irrigation pipeline: f–j; and 3-D volumes: k–o) observed during and after the irrigation phase (Table 1), compared to the initial condition (no irrigation), in T1 and T2. A value of 100% indicates no change in ER terms with respect to the initial condition; values higher and lower than 100% indicate increases (drying patterns) and decreases of ER (wetting patterns), respectively. Both in T1 and T2, the main phenomenon occurring within the explored ERT volume was an ER ratio decreasing (soil wetting patterns), even if localized areas (less than 1% of the overall explored volume) were characterized by ER increasing (drying patterns) with respect to the initial condition (Table 1).

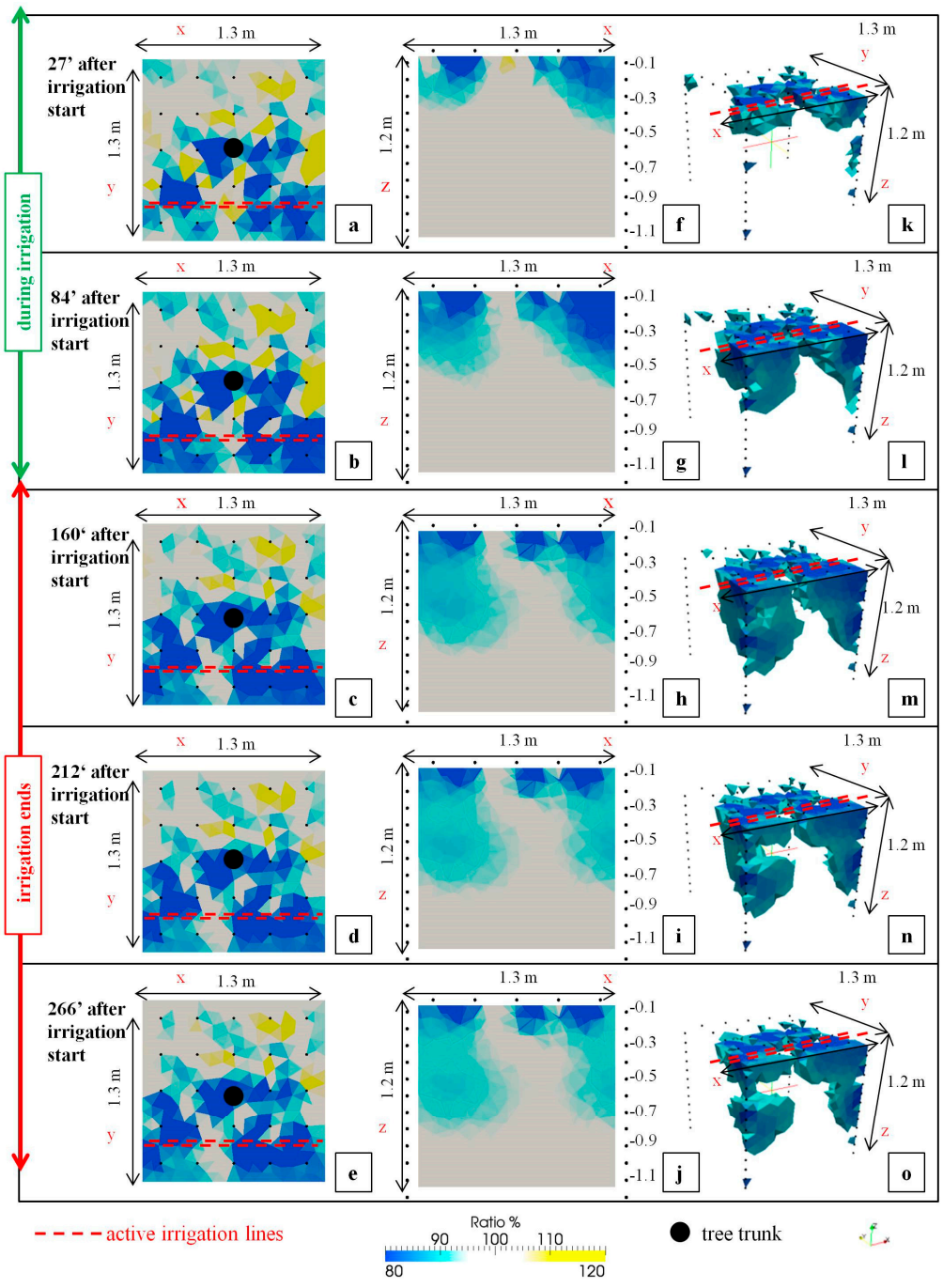

Figure 5. Time-lapse electrical resistivity (ER) ratio imagery (at the surface: **a–e**; transects under the irrigation pipeline: **f–j**; and 3-D volumes: **k–o**) for T1 with respect to the initial condition (no irrigation).

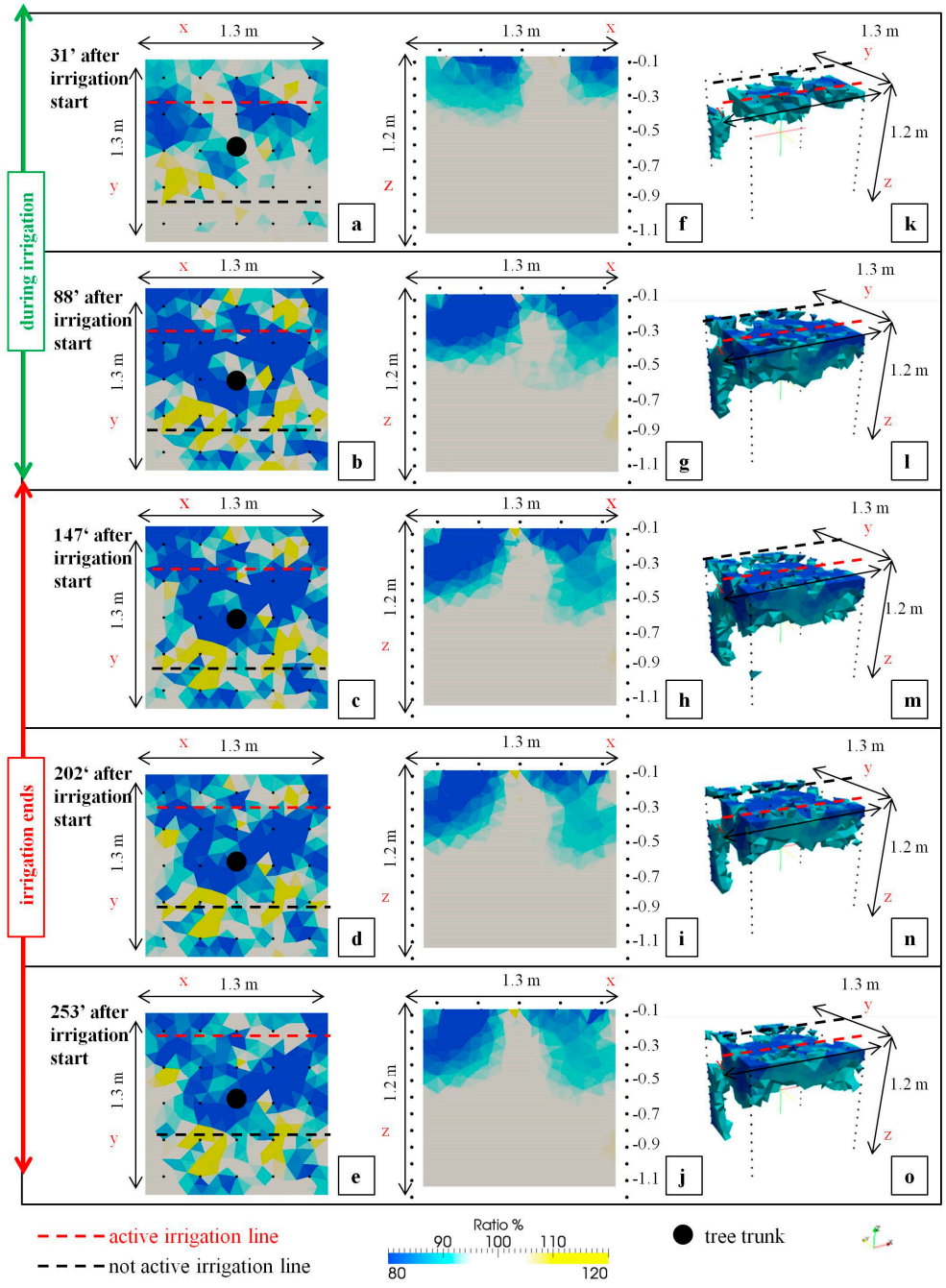

Figure 6. Time-lapse electrical resistivity (ER) ratio imagery (at the surface: **a**–**e**; transects under the irrigation line: **f**–**j**; and 3-D volumes: **k**–**o**) for T2 with respect to the initial condition (no irrigation).

Figure 2a shows the evolution of the exposed wetted area (f_{ew}) during and after the irrigation phase in T1 and T2. The mean f_{ew} value obtained from both T1 and T2 was 0.1. This value was used for running the SWB model within the ERT-adjusted dual K_c FAO-56 approach.

At the surface level, the main ER decreasing patterns are localized close to the active irrigation pipeline, both T1 and T2, during the irrigation phase (Figure 5a,b, Figure 6a,b and Figure 2a). Nevertheless, once the irrigation phase finished (after about 88 min from the irrigation start, Table 1), patterns in ER decreasing are always observed (time 03, Figures 5c, 6c and 2a). At times 04–05 (Table 1, Figure 2a) the same patterns became quite steady showing a slight increase.

Figure 2b shows the evolution of the infiltration front depth (m) during and after the irrigation phase in T1 and T2. Analyzing the ER changes from the top soil to the bottom-layer (Figures 5f–j

and 6f–j), two phases were identified. During the irrigation phase, an increase of the infiltration front depth was observed both in T1 and T2, but with different magnitudes. In fact, in T1, where the full irrigation is applied, the wetting patterns distribution reached greater depths than T2 (supplied at 50% in respect to T1 irrigation rate) with a maximum of 0.8 and 0.6 m, respectively. After the irrigation end, the infiltration front remained almost constant or even evidenced a slight depth reduction (Figure 5f–j, Figures 6f–j and 2b).

At 3-D level (Figures 5k–o and 6k–o), during the irrigation phase (times 01 and 02 in Table 1; and Figure 5k,l and Figure 6k,l), a marked decrease in ER ratio (values equal to or less than 90%) was observed. ER reductions ranged from 5% to 16% on average of the overall explored volume in T1 and T2, due to progression of the irrigation front in correspondence with the active irrigation pipelines (2 drip irrigation emitters on the surface of T1 and T2 within the ERT explored volume). After the irrigation phase (time 03 in Table 1; and Figures 5m and 6m), the wetting volumes became quite stable, around 16% of the total volume, followed by a slight decrease until 12–13% (times 04 and 05 in Table 1; and Figures 5n–o and 6n–o).

3.3. Satellite dual Kc Approach

3.3.1. Maps of original and ERT-adjusted dual K_c FAO-56

Figure 7 shows an example of spatially distributed estimates of dual K_c ($K_{c,FAO}$ and $K_{c,ERT}$; a,b) and ET (ET_{FAO} and ET_{ERT}; c,d) obtained for the study area by the original and ERT-adjusted dual K_c FAO-56 approach for DOY 193 (under ET_0 conditions of 8.56 mm day^{-1}). The dual K_c values derived from FAO-56 and ERT-adjusted approaches were 0.69 and 0.59, respectively, resulting in ET values of 5.91 (ET_{FAO}) and 5.06 mm (ET_{ERT}).

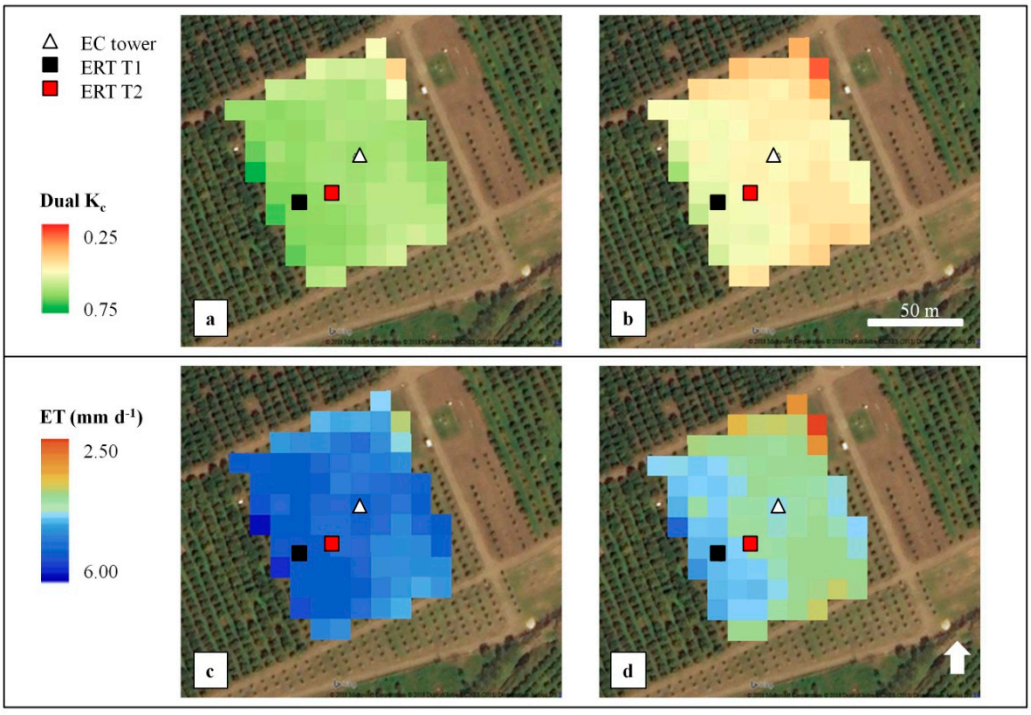

Figure 7. Dual crop coefficient ($K_{c,FAO}$ and $K_{c,ERT}$; **a**,**b**) and ET (ET_{FAO} and ET_{ERT}; **c**,**d**) estimates obtained by the original and ERT-adjusted dual K_c FAO-56 approach for DOY 193 (under ET_0 conditions of 8.56 mm day^{-1}).

3.3.2. ET Comparison: Original and ERT-Adjusted Dual K_c FAO-56 vs EC

Figure 8 shows the scatterplot between the daily measured ET_{EC}, the original (ET_{FAO}), and the ERT-adjusted (ET_{ERT}) dual K_c FAO-56 approaches satellite ET estimates.

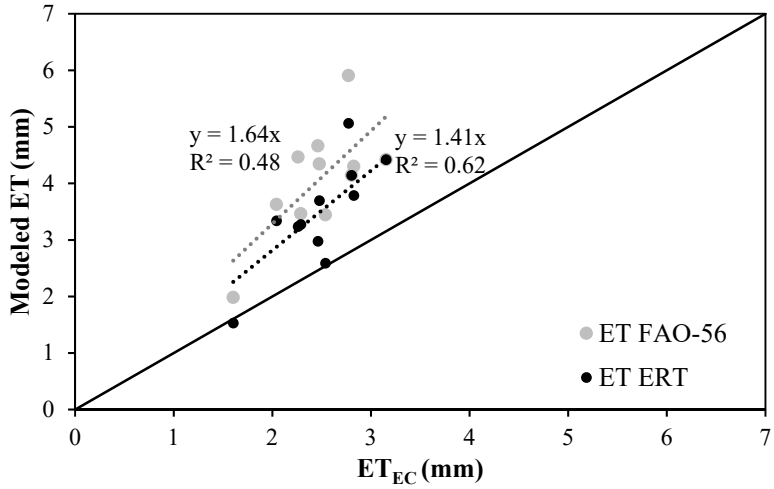

Figure 8. Comparison between modelled ET_{FAO} and ET_{ERT} versus measured ET_{EC}. The black solid line represents the 1:1 relationship.

Daily modelled ET values (ET_{FAO} and ET_{ERT}, with average values of 4.07 and 3.46 mm, respectively) resulted in an average 64% and 40% greater than the measured ET_{EC} fluxes (average value of 2.47 mm), with root mean square errors (RMSE) of 1.74 and 1.17 mm day^{-1} and coefficients of determination (R^2) of 0.48 and 0.62, respectively. The slope terms were 1.64 and 1.41 for ET_{FAO} and ET_{ERT} respectively, reflecting that ET discrepancies with respect to ET_{EC} were greater for high ET values. The average T component was 3.19 mm for both original and ERT-adjusted dual K_c FAO-56 approaches, whereas E term was 0.88 mm and 0.27 mm, respectively.

3.3.3. Crop Coefficients Comparison and K_s Estimation

Figure 9 shows the crop coefficients (K_{cb} + K_e) obtained from EC ($K_{c,EC}$) and from the original ($K_{c,FAO}$) and ERT-adjusted ($K_{c,ERT}$) dual K_c FAO-56 approaches. Within the reference period (June–September 2017), the observed K_c using EC ($K_{c,EC}$) was 0.40 ± 0.08. For the same period, $K_{c,FAO}$ and $K_{c,ERT}$ resulted in 0.64 ± 0.12 and 0.54 ± 0.11, respectively.

Temporal evolution of water stress coefficient (K_s) obtained as Equation (13) is reported in Figure 9. K_s values ranged from 0.55 to 1.00 with an average of 0.74.

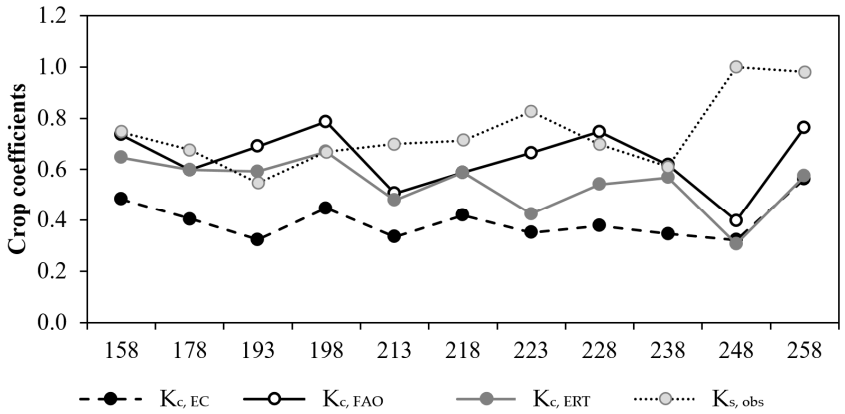

Figure 9. K_c from EC ($K_{c,EC}$) and from the original ($K_{c,FAO}$) and ERT-adjusted dual K_c FAO-56 approach ($K_{c,ERT}$), and K_s derived from ET_{EC} and ET_{ERT} ratio.

4. Discussion

The need of accurate ET estimates from remote sensing data calls for simplified methods to be applied at a wide range of spatial resolutions [38]. The lack of useful applications may be overcome

by combining different multi-platforms data [39] or by using modelling [40,41], as in this study, by combining remote sensing data with geophysical information.

The most remarkable features of the ERT time-lapse inversions in Figures 5 and 6 are the decreasing of ER ratio (wetting patterns) that seem to change substantially over time. As irrigation occurs in a very contained portion of the area monitored by ERT, it is not surprising that ER tends to decline largely in correspondence to drippers activity, creating consistent soil wetting patterns that extend from the surface to the bottom of the monitored soil volume (1.2 m depth) during irrigation and tends to become steady or decrease at the end of the irrigation phase (Figures 5 and 6). The different magnitude of these changes among treatments at localized depths is explained by the different irrigation rates applied in T1 (full irrigation) and T2 (deficit irrigation under PRD). Drying patterns (increasing of ER ratio) observed close to the surface can be attributed to direct evaporation from the top soil or root-water-uptake processes [22] or to inversion artefacts [42]. Due to the complexity of the hydrological processes that act within the soil-root system, an integration of hydrological and geophysical modelling might improve the analysis of recorded ER patterns [43].

The f_{ew} information retrieved using ERT were herein included in the adjusted satellite dual K_c FAO-56 approach. The obtained results showed that ERT improved ET estimates (and E), with respect to the estimates obtained by the original dual K_c FAO-56 approach, when compared with the site-specific ET_{EC} rates measured at the experimental site by EC. In fact, the comparison between $K_{c,FAO}$ and $K_{c,ERT}$ reveals that $K_{c,ERT}$ was always lower than $K_{c,FAO}$, this discrepancy being due to the more accurate estimation of f_{ew} performed in the ERT-adjusted approach. Consequently, with the ERT-adjusted approach, the E term, and therefore ET, was considerably reduced (15%) when compared with the original dual K_c FAO-56 approach [14]. Nevertheless, ET obtained from both approaches, even considering the ERT-adjustment, remained substantially higher than ET measured in EC (64% and 40%, respectively). Such overestimations could be due to the assumption taken in this study of considering f_{ew} constant during the day, since it is well known that f_{ew} progressively diminish after an irrigation event. Additionally, the presence of different irrigation treatments within the footprint of the EC tower may introduce some uncertainties in the results obtained. In addition, the spatial resolution of Sentinel does not allow the separation of regions irrigated differentially. Therefore, this limitation could be solved by using high spatial resolution images, such as those acquired by unmanned aerial vehicles, which would allow the f_{ew} of each irrigation treatment to be considered separately instead of averaging both of them, as done for mixed pixels. Similar to the results obtained in this study, several authors have found ET overestimation ranging from 12% to 42% when comparing ET from the FAO 56 approach with ET provided by EC in heterogeneous orchards under drip irrigation [44,45] indicating that the overestimation was even worse when examining only the irrigated period [46]. These authors pointed out that the values of K_{cb} suggested by [14,45,46] and the high soil evaporation predicted following the FAO-56 approach [45,46] as the main reasons for these overestimations. In general, the magnitude of such overestimations was lower than the one obtained in this study probably due to the water stress expected in our experiment as consequence of the deficit irrigation conditions applied at the experimental site. Deficit irrigation strategy played a strategic role in altering the normal ratio between the energy balance surface fluxes, determining a fairly high sensible heat flux and an ET reduction or underestimation due to the imposed water stress conditions [31]. This behavior was poorly captured by the original and the ERT-adjusted K_c FAO-56 approaches, whereas it was taken into account in the ET_{EC} value obtained using the EC technique, as indicated by the calculated K_s ($\approx$0.74).

Despite the good results obtained using 3-D ERT for helping to estimate ET, future developments of this technique should attempt for speed operational applications (e.g., the need for real time data). Additionally, future research should address the mid–long term temporal evolution of f_{ew} to better characterize changes in soil water conditions and subsequently evaporation, in order to incorporate dynamic f_{ew} values into the approach instead of using a constant one. At this stage, ERT may be considered a useful tool for precision irrigation strategies, in particular for identifying the soil wetting patterns distribution and also allowing a better characterization of the wet bulb, which may therefore

improve the efficiency of irrigation [21]. Currently, the scope of ERT is limited to scientific research or as a validation method for calibrating other methods that can be more easily incorporated into the daily activities of farmers and technicians. In the future, more commercially oriented applications of ERT technologies could be derived in order to facilitate the implementation of this technique for agriculture water management applications.

5. Conclusions

The main conclusions to be drawn from this study can be summarized as follows:

- Spatially distributed ET rates can be obtained by incorporating VI_s computed using remote sensing technologies into the dual K_c FAO-56 approach.
- The integration of 3-D ERT methodology into the dual K_c FAO-56 approach considerably reduced errors in ET estimates. This technology allowed the tracking of the wetting distribution patterns, helping to accurately estimate f_{ew} and therefore the water evaporated from the soil surface.
- The dual K_c FAO-56 approach determines ET under standard conditions where no limitations are placed on crop growth or ET, whereas EC measures ET even for non-standard conditions (e.g., under soil water stress conditions). From the comparison between the ET measured from the EC tower and the ET estimated from the ERT-adjusted dual K_c FAO-56 approach, the K_s term can be experimentally derived.

Author Contributions: The authors contributed with equal effort to the realization of the study.

Funding: The authors thank the EU, the Italian Ministry of Education, Universities and Research, and the Spanish Agencia Estatal de Investigación for funding, as part of the collaborative international consortium IRIDA ("Innovative remote and ground sensors, data and tools into a decision support system for agriculture water management"), financed under the ERA-NET Cofund WaterWorks 2014. This ERA-NET is an integral part of the 2015 Joint Activities developed by the Water Challenges for a Changing World Joint Programme Initiative (Water JPI). The authors also acknowledge support from the ERANET-MED project WASA ("Water Saving in Agriculture: Technological developments for the sustainable management of limited water resources in the Mediterranean area").

Acknowledgments: The authors wish to thank Servizio Informativo Agrometeorologico Siciliano (SIAS) for weather data and the personnel of Centro di Ricerca Olivicoltura, Frutticoltura e Agrumicoltura of the Italian Council for Agricultural Research and Agricultural Economics Analyses (CREA-OFA, Acireale) for their hospitality at the experimental site.

Conflicts of Interest: The authors declare no conflicts of interest. The funders had no role in the design of the study; in the collection, analyses, or interpretation of data; in the writing of the manuscript, and in the decision to publish the results.

References

1. French, R.J.; Schultz, J.E. Water use efficiency of wheat in a Mediterranean type environment. I. The relation between yield, water use and climate. *Aust. J. Agric. Res.* **1984**, *35*, 743–764. [CrossRef]
2. French, R.J.; Schultz, J.E. Water use efficiency of wheat in a mediterranean-type environment. II. Some limitations to efficiency. *Aust. J. Agric. Res.* **1984**, *35*, 765–775. [CrossRef]
3. Capra, A.; Consoli, S.; Russo, A.; Scicolone, B. Integrated agro-economic approach to deficit irrigation on lettuce crops in Sicily (Italy). *J. Irrig. Drain. Eng.* **2008**, *134*, 437–445. [CrossRef]
4. Consoli, S.; Papa, R. Corrected surface energy balance to measure and model the evapotranspiration of irrigated orange orchards in semi-arid Mediterranean conditions. *Irrig. Sci.* **2013**, *31*, 1159–1171. [CrossRef]
5. Zhao, P.; Kang, S.; Li, S.; Ding, R.; Tong, L.; Du, T. Seasonal variations in vineyard ET partitioning and dual crop coefficients correlate with canopy development and surface soil moisture. *Agric. Water Manag.* **2018**, *197*, 19–33. [CrossRef]
6. Yau, S.K.; Nimah, M.; Farran, M. Early sowing and irrigation to increase barley yields and water use efficiency in Mediterranean conditions. *Agric. Water Manag.* **2011**, *98*, 1776–1781. [CrossRef]

7. Yan, A.; Gao, C.; Ren, Y.; Zong, R.; Ma, Y.; Li, Q. Effects of pre-sowing irrigation and straw mulching on the grain yield and water use efficiency of summer maize in the North China Plain. *Agric. Water Manag.* **2017**, *186*, 21–28. [CrossRef]
8. Eastham, J.; Gregory, P.J.; Williamson, D.R.; Watson, G.D. The influence of early seeding of wheat and lupin crops on evapotranspiration and evaporation from the soil surface in a Mediterranean climate. *Agric. Water Manag.* **1999**, *42*, 205–218. [CrossRef]
9. Liu, C.M.; Zhang, X.Y.; Zhang, Y.Q. Determination of daily evaporation and evapotranspiration of winter wheat and maize by large-scale weighing lysimeter and micro-lysimeter. *Agric. For. Meteorol.* **2002**, *111*, 109–120. [CrossRef]
10. Photiades, A.; Hadjichristodoulou, A. Sowing date, sowing depth, seed rate and row spacing of wheat and barley under dryland conditions. *Field Crops Res.* **1984**, *9*, 151–162. [CrossRef]
11. Lascano, R.J.; Baumhardt, R.L.; Hicks, S.K.; Heilman, J.L. Soil and plant water evaporation from strip-tillage control, measurement and simulation. *Agron. J.* **1994**, *86*, 987–994. [CrossRef]
12. Stagnari, F.; Galieni, A.; Speca, S.; Cafiero, G.; Pisante, M. Effects of straw mulch on growth and yield of durum wheat during transition to Conservation Agriculture in Mediterranean environment. *Field Crops Res.* **2014**, *167*, 51–63. [CrossRef]
13. Prosdocimi, M.; Jordan, A.; Tarolli, P.; Keesstra, S.; Novara, A.; Cerda, A. The immediate effectiveness of barley straw mulch in reducing soil erodibility and surface runoff generation in Mediterranean vineyards. *Sci. Total Environ.* **2016**, *547*, 323–330. [CrossRef] [PubMed]
14. Allen, R.G.; Pereira, L.S.; Raes, D.; Smith, M. *Crop Evapotranspiration-Guidelines for Computing Crop Water Requirements-FAO Irrigation and Drainage Paper 56*; FAO: Rome, Italy, 1998; Volume 300, p. D05109.
15. González-Dugo, M.P.; Neale, C.M.U.; Mateos, L.; Kustas, W.P.; Prueger, J.H.; Anderson, M.C.; Li, F. A comparison of operational remote sensing-based models forestimating crop evapotranspiration. *Agric. For. Meteorol.* **2009**, *149*, 1843–1853. [CrossRef]
16. Subbaiah, R. A review of models for predicting soil water dynamics during trickle irrigation. *Irrig. Sci.* **2013**, *31*, 225–258. [CrossRef]
17. Jarvis, N.; Koestel, J.; Larsbo, M. Understanding preferential flow in the vadose zone: Recent advances and future prospects. *Vadose Zone J.* **2016**, *15*, 15. [CrossRef]
18. Hardie, M.; Ridges, J.; Swarts, N.; Close, D. Drip irrigation wetting patterns and nitrate distribution: Comparison between electrical resistivity (ERI), dye tracer, and 2D soil–water modelling approaches. *Irrig. Sci.* **2018**, *36*, 97–110. [CrossRef]
19. Cassiani, G.; Boaga, J.; Vanella, D.; Perri, M.T.; Consoli, S. Monitoring and modelling of soil–plant interactions: The joint use of ERT, sap flow and eddy covariance data to characterize the volume of an orange tree root zone. *Hydrol. Earth Syst. Sci.* **2015**, *19*, 2213–2225. [CrossRef]
20. Cassiani, G.; Boaga, J.; Rossi, M.; Putti, M.; Fadda, G.; Majone, B.; Bellin, A. Soil–plant interaction monitoring: Small scale example of an apple orchard in Trentino, North-eastern Italy. *Sci. Total Environ.* **2016**, *543*, 851–861. [CrossRef]
21. Consoli, S.; Stagno, F.; Vanella, D.; Boaga, J.; Cassiani, G.; Roccuzzo, G. Partial root-zone drying irrigation in orange orchards: Effects on water use and crop production characteristics. *Eur. J. Agron.* **2017**, *82*, 190–202. [CrossRef]
22. Vanella, D.; Cassiani, G.; Busato, L.; Boaga, J.; Barbagallo, S.; Binley, A.; Consoli, S. Use of small scale electrical resistivity tomography to identify soil-root interactions during deficit irrigation. *J. Hydrol.* **2018**, *556*, 310–324. [CrossRef]
23. Binley, A.M.; Kemna, A. DC resistivity and induced polarization methods. In *Hydrogeophysics*; Rubin, Y., Hubbard, S.S., Eds.; Springer: Dordrecht, The Netherlands, 2005; Volume 50, pp. 129–156. [CrossRef]
24. Binley, A. Tools and techniques: DC electrical methods. In *Treatise on Geophysics*, 2nd ed.; Schubert, G., Ed.; Elsevier: Amsterdam, The Netherlands, 2015; Volume 11, pp. 233–259. [CrossRef]
25. Consoli, S.; Vanella, D. Comparisons of satellite-based models for estimating evapotranspiration fluxes. *J. Hydrol.* **2014**, *513*, 475–489. [CrossRef]
26. Consoli, S.; Vanella, D. Mapping crop evapotranspiration by integrating vegetation indices into a soil water balance model. *Agric. Water Manag.* **2014**, *143*, 71–81. [CrossRef]
27. Huete, A.R. A soil-adjusted vegetation index (SAVI). *Remote Sens. Environ.* **1988**, *25*, 295–309. [CrossRef]

28. Gutman, G.; Ignatov, A. The derivation of the green vegetation fraction from NOAA/AVHRR data for use in numerical weather prediction models. *Int. J. Remote Sens.* **1998**, *19*, 1533–1543. [CrossRef]
29. Rouse, J.W.; Haas, R.H.; Schell, J.A.; Deering, D.W.; Harlan, J.C. *Monitoringthe Vernal Advancement and Retrogradation of Natural Vegetation*; Type III, Final Report; NASA/GSFC: Greenbelt, MD, USA, 1974; pp. 1–371.
30. Consoli, S.; Stagno, F.; Roccuzzo, G.; Cirelli, G.; Intrigliolo, F. Sustainable management of limited water resources in a young orange orchard. *Agric. Water Manag.* **2014**, *132*, 60–68. [CrossRef]
31. Vanella, D.; Consoli, S. Eddy Covariance fluxes versus satellite-based modelisation in a deficit irrigated orchard. *Ital. J. Agrometeorol.* **2018**, *2*, 41–52. [CrossRef]
32. Aiello, R.; Bagarello, V.; Barbagallo, S.; Consoli, S.; Di Prima, S.; Giordano, G.; Iovino, M. An assessment of the Beerkan method for determining the hydraulic properties of a sandy loam soil. *Geoderma* **2014**, *235*, 300–307. [CrossRef]
33. Baldocchi, D.D. Assessing the eddy covariance technique for evaluating carbon dioxide exchange rates of ecosystems: Past, present and future. *Glob. Chang. Biol.* **2003**, *9*, 479–492. [CrossRef]
34. Aubinet, M.; Grelle, A.; Ibrom, A.; Rannik, U.; Moncrieff, J.; Foken, T.; Kowalski, A.S.; Martin, P.H.; Berbigier, P.; Bernhofer, C.; et al. Estimates of the annual net carbon and water exchange of European forests: The EUROFLUX methodology. *Adv. Ecol. Res.* **2000**, *30*, 113–175.
35. Kaimal, J.C.; Finnigan, J.J. *Atmospheric Boundary-Layer Flows: Their Structure and Measurement*; Oxford University Press: Oxford, UK, 1994; 289p.
36. Prueger, J.H.; Hatfield, J.L.; Kustas, W.P.; Hipps, L.E.; MacPherson, J.I.; Parkin, T.B. Tower and aircraft eddy covariance measurements of water vapor, energy and carbon dioxide fluxes during SMACEX. *J. Hydrometeorol.* **2005**, *6*, 954–960. [CrossRef]
37. Twine, T.E.; Kustas, W.P.; Norman, J.M.; Cook, D.R.; Houser, P.; Meyers, T.P.; Prueger, J.H.; Starksh, P.J.; Wesely, M.L. Correcting eddy-covariance flux underestimates over a grassland. *Agric. For. Meteorol.* **2000**, *103*, 279–300. [CrossRef]
38. Wang, K.; Liang, S. An improved method for estimating global evapotranspiration based on satellite determination of surface net radiation, vegetation index, temperature, and soil moisture. *J. Hydrometeorol.* **2008**, *9*, 712–727. [CrossRef]
39. Knipper, K.; Hogue, T.; Scott, R.; Franz, K. Evapotranspiration estimates derived using multi-platform remote sensing in a semiarid region. *Remote Sens.* **2017**, *9*, 184. [CrossRef]
40. Sun, G.; Alstad, K.; Chen, J.; Chen, S.; Ford, C.R.; Lin, G.; Liu, C.; Lu, N.; McNulty, S.G.; Miao, H.; et al. A general predictive model for estimating monthly ecosystem evapotranspiration. *Ecohydrology* **2011**, *4*, 245–255. [CrossRef]
41. Consoli, S.; Licciardello, F.; Vanella, D.; Pasotti, L.; Villani, G.; Tomei, F. Testing the water balance model criteria using TDR measurements, micrometeorological data and satellite-based information. *Agric. Water Manag.* **2016**, *170*, 68–80. [CrossRef]
42. Kim, J.H.; Yi, M.J.; Park, S.G.; Kim, J.G. 4-D inversion of DC resistivity monitoring data acquired over a dynamically changing earth model. *J. Appl. Geophys.* **2009**, *68*, 522–532. [CrossRef]
43. Busato, L.; Boaga, J.; Perri, M.T.; Majone, B.; Bellin, A.; Cassiani, G. Hydrogeophysical characterization and monitoring of the hyporheic and riparian zones: The Vermigliana Creek case study. *Sci. Total Environ.* **2018**, *648*, 1105–1120. [CrossRef]
44. Paço, T.A.; Ferreira, M.I.; Conceição, N. Peach orchard evapotranspiration in a sandy soil: Comparison between eddy covariance measurements and estimates by the FAO 56 approach. *Agric. Water Manag.* **2006**, *85*, 305–313. [CrossRef]
45. Er-Raki, S.; Chehbouni, A.; Guemouria, J.; Ezzahar, J.; Khabba, S.; Boulet, G.; Hanich, L. Citrus orchard evapotranspiration: Comparison between eddy covariance measurements and the FAO-56 approach estimates. *Plant Biosyst.* **2009**, *143*, 201–208. [CrossRef]
46. Maestre-Valero, J.F.; Testi, L.; Jiménez-Bello, M.A.; Castel, J.R.; Intrigliolo, D.S. Evapotranspiration and carbon exchange in a citrus orchard using eddy covariance. *Irrig. Sci.* **2017**, *35*, 397–408. [CrossRef]